Structural Changes to Supported Water Nanoislands Induced by Kosmotropic Ions

Irene Weber,*,† Nikki Gerrard,‡ Andrew Hodgson,‡ and Karina Morgenstern†

†*Lehrstuhl für physikalische Chemie I, Ruhr-Universität Bochum, Universitätsstraße 150, D-44801 Bochum, Germany*

‡*Surface Science Research Centre, University of Liverpool, Liverpool L69 3BX, United Kingdom*

E-mail: irene.weber@rub.de

Abstract

We report on the influence of lithium ions on binding and structure of water nanoislands on Au(111) by temperature-programmed desorption and variable-temperature scanning tunneling microscopy. Water coverages between a fraction and a full bilayer and two lithium coverages (< 0.15 % ML) are explored. Lithium enhances selectively the binding of some of the water molecules on precovered Au(111) as compared to water on pristine Au(111); revealed by an increase of the water desorption temperature by approx. 10 K. Surprisingly, the effect of lithium on the structure of water is much more extended than expected from these desorption experiments. A small amount of lithium changes the structure of water nanoislands drastically compared to those on pristine Au(111). On pristine Au(111), water ice grows in the form of crystalline islands that are 2 or 3 bilayers high. On Li precovered Au(111), the islands are more corrugated, at a five times broader apparent height distribution, and much smaller, at a four times smaller area distribution. These changes reflect the influence of lithium as

a structure-maker, or kosmotrope, on water. Our study provides unprecedented real-space information of the influence of a kosmotrope on water structure at the nanoscale. We utilize its kosmotropic behaviour to provide real-space images of desorption.

Introduction

The interaction of ions with water molecules is not only of fundamental interest for electrochemistry,[1] electrocatalysis[2] and energy storage[3] but also important for atmospheric[4] and biological processes.[5,6] Up to now, ion-water interaction has been studied experimentally mainly in the liquid[7–10] and the gas phase[11–15] but rarely in the solid phase.[16–20] A microscopic understanding has been developed in theory by molecular dynamics (MD) simulations[21,22] and by density functional theory (DFT) calculations.[10,14,20,23–25]

On the other hand, the microscopic understanding of water self-interactions has progressed substantially through real space imaging of supported ice at cryogenic temperatures.[26–29] From these studies, the structure of ice on a multitude of metal surfaces is known on a molecular level, including the here investigated Au(111).[30,31] We probe Au(111), because it is one of the most important electrodes in electrochemistry. On Au(111), the structure of D_2O monomers and small clusters have been analyzed in real space at 25 K.[32] Also for larger coverages, adsorption of H_2O on Au(111) was only explored at 20 K[33] and not at the temperatures of our study. Helium scattering revealed that at these higher temperatures between 110 K and 130 K water is crystalline.[34] What remains to be explored is how the structure of water nanoislands is affected by ions to acquire a microscopic understanding of water-ion interaction. This is of utmost importance for all the above mentioned processes.

To understand the water-ion interaction, we explore lithium ions, which due to their small size have the largest effect on the structure of the surrounding water.[35] Such alkali metals are known to ionize on metal surfaces, e.g. sodium on Cu(001).[36] These and other properties of alkali metals on metal surfaces were well characterized by vibrational spectroscopy and ab-initio theoretical analysis.[37]

The interaction of lithium with water has so far been investigated only in gas and fluid phase. In the gas phase, lithium is surrounded by three water molecules in the first solvation shell.[15] In the fluid phase, the interaction of lithium with water is usually characterized as a kosmotrope, i.e. as a structure maker, which changes the structure of water beyond the ion's first hydration shell by enhancing hydrogen bonding of the water as compared to bulk water.[35]

Very little is known about the interaction of ions with water on surfaces. While the interaction of lithium with water has not yet been studied on a surface to our knowledge, sodium, another kosmotrope, has been explored on Ru(0001).[16] Electron stimulated desorption ion angular distributions (ESDIAD) demonstrated that sodium changes water orientation in its vicinity. For the chaotrope or structure breaker potassium on Pt(111), temperature-programmed desorption (TPD) suggested a breaking of the water bilayer structure.[17] What has not yet been investigated is the real-space structure of solvent-ion complexes.

In this article, we investigate the influence of lithium ions on water ice supported on Au(111) by means of scanning tunneling microscopy (STM) and TPD. After characterizing the two systems separately, the pure water and the pure Li on pristine Au(111), we compare our results to water structure and binding on Li precovered Au(111) at two different Li coverages. Both, TPD and STM measurements reveal substantial differences. Our real-space results may alter the way of thinking about the structure of solvent-ion complexes.

Methods

The STM measurements are performed in a ultrahigh vacuum (UHV) chamber with a base pressure of 4×10^{-10} mbar. The chamber is equipped with a commercial single-tube scanner variable-temperature STM (105 K - 350 K), a quadrupole mass-spectrometer, an evaporator for deposition of alkali metals and a molecular deposition unit to deposit D_2O. The single-crystalline Au(111) surface is cleaned by several cycles of Ar^+ ion sputtering at 1.3 keV

($p_{\mathrm{argon}} = 3.8 \times 10^{-5}$ mbar, $I_{\mathrm{sputter}} = 9.6$ μA, $t = 15$ - 30 min) followed by annealing at 850 K by electron bombardment ($I_{\mathrm{emission}} = 13.6$ mA, $V_{\mathrm{accelerating}} = 1$ kV, $t = 10$ - 30 min). The cleanliness of the sample is checked by STM. One control experiment is performed in a low temperature STM (for experimental details see[28]).

The TPD experiments are performed in another UHV chamber with a base pressure of 3×10^{-11} mbar. The chamber is equipped with a quadrupole mass-spectrometer, a Low Energy Electron Diffraction (LEED), an evaporator for alkali metals and a molecular beam doser for water dosing. The single-crystalline Au(111) surface is cleaned by several cycles of Ar^+ ion sputtering at 0.5 eV ($p_{\mathrm{argon}} = 7.3 \times 10^{-6}$ mbar, $I_{\mathrm{sputter}} = 5.4\mu$A, $t = 10$ - 30 min) and annealing at 900 K by direct heating ($I_{\mathrm{heat}} = 19.6$ A, $V_{\mathrm{heat}} = 2.6$ V, $t = 10$ min). The cleanliness is checked by LEED and TPD until the LEED pattern of the herringbone reconstruction appears bright and the background black and until only one characteristic peak of D_2O at 154 K is detected in the TPD spectrum.

In both chambers, D_2O of milli-q quality is further cleaned in vacuum through freeze-pump-thaw cycles and the SAES alkali-metal dispenser is degassed before first evaporation ($T = 1200$ K, $t = 2$ min). For the TPD experiment, lithium is deposited on Au(111) at (220 $\pm$ 10) K, ($T_{\mathrm{dispenser}} = 1100$ K, $t = 30$ sec). D_2O is dosed on the surface held at (100 $\pm$ 1) K, (110 $\pm$ 1) K and (130 $\pm$ 1) K with a rate of 0.1 BL min^{-1} using an effusive, low pressure molecular beam with two stages of differential pumping. The beam forms a spot on the surface with a diameter of 5 mm. In the STM experiment, the Au(111) is held at (215 $\pm$ 5) K during lithium adsorption ($T_{\mathrm{dispenser}} = 950$ K, $t = 17$ sec). The adsorption is repeated 2 or 4 times. As the lithium is mobile at measurement temperature (see main text) unless it is bound to the elbows of the herringbone reconstruction of Au(111) or the step edges, we are only able to give lower limits of the coverage, which are 0.9×10^{-4} ML and 1.5×10^{-4} ML. D_2O is deposited with a rate of 1 BL min^{-1}; the sample is held at (115 $\pm$ 5) K.

TPD spectroscopy is performed at a heating rate of (0.3 $\pm$ 0.1) K/s for pure D_2O on Au(111) and (0.4 $\pm$ 0.1) K/s for D_2O on lithium covered Au(111). The crystal is held by two Ta

heating wires which are spot welded to high current feed-throughs mounted at the base of a liquid nitrogen coolable manipulator. The temperature is measured by a chromel-alumel thermocouple fitting into a hole at the side of the crystal. With this arrangement, the crystal can be heated or cooled rapidly, with minimal desorption from the support. Combined with molecular beam dosing, the TPD spectra are free from edge or support effects. As there is no monolayer peak in the TPD spectrum of water on pristine Au(111)[38] the area of the monolayer peak of D_2O on Cu(511) is used to calibrate the flux of the molecular beam doser and thus determine the D_2O coverage.[39]

The apparent height of water islands measured by STM is determined using WSxM, a free-ware program from Nanotec Electronica S.L..[40] Because of the corrugation of Au(111), heights are given as the difference between the mean of the surface values and the mean of the island values. The volume of the islands is estimated as a product of the area of the D_2O islands determined using WSxM and the numbers of D_2O bilayers derived from apparent heights according to the results for D_2O islands on Cu(111).[28]

Results and Discussion

Water adsorption on pristine Au(111).

In order to set the stage for investigating the influence of the ions on water binding and structure, we first characterize water structures on and desorption dynamics from pristine Au(111), i.e. without ions, under the conditions of water exposure that we use in our study.

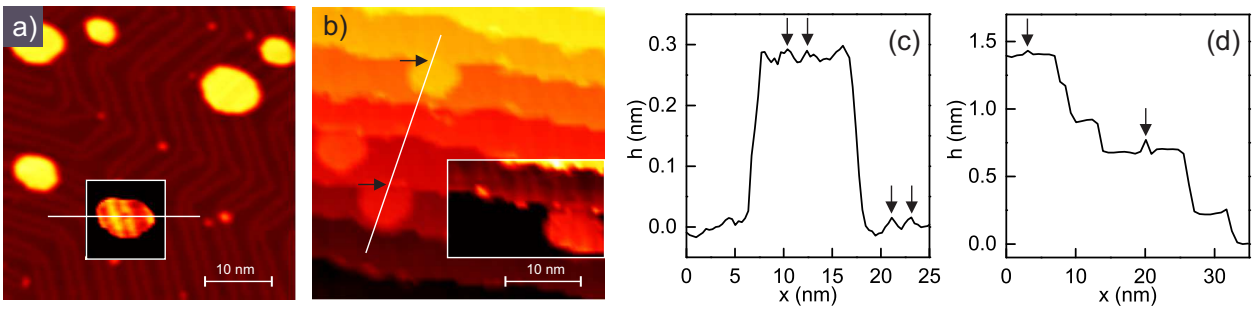

Figure 1: Water islands on Au(111) grown at (115 ± 5) K (0.26 BL): STM image of (a) terrace region; contrast is enhanced in rectangle, 30 pA, 280 mV, T = (127 ± 1) K (b) stepped region; contrast is enhanced in rectangle, 60 pA, 280 mV, T = (125 ± 1) K (c) line scan crossing the herringbone reconstruction as indicated in (a); arrows point to the domain boundaries of the herringbone reconstruction (d) line scan crossing the stepped regions as indicated in (b); arrows point to higher imaged edge; for high-resolution images of insets see supporting information.

Due to a slight misorientation, low-indexed faces of crystals have an intrinsic number of surface steps. For the best available surface orientation of $<0.1\ ^{o}$ used here, this results in up to 200 steps/μm. While such steps are equally distributed at annealing temperatures on Au(111), they tend to form two regions at room temperature and below, regions with large terraces, and regions with an equilibrium step distance of (5.1 ± 0.6) nm, in our case.
On both surface regions, water adsorbed at (115 ± 5) K forms islands (Fig. 1). On terraces, small islands decorate the elbow sites of the herringbone reconstruction, but larger islands are also nucleated homogeneously. This homogeneous nucleation is demonstrated in Fig. 1a, where some islands are not situated at the elbow sites of the herringbone reconstruction, but are randomly distributed over the surface. In stepped regions of the surface, there are no elbow sites. Here, small islands nucleate at the intersection of the domain boundaries with the step edge (Fig. 1b, enhanced contrast); large islands nucleate at the lower step edge in the fcc region (Fig. 1b). For small terraces, some water islands extend over the whole terrace at the chosen coverage (Fig. 1b, lower left). Note that the apparent heights of the water islands are in the range of the interlayer distance of Au(111), at 0.24 nm (Fig. 1d), but, they are distinguished by a higher imaged edge that is indicated by the arrows in Fig. 1b and 1d.

He-scattering revealed, at the same adsorption and measurement temperature, well-ordered islands with a $(\sqrt{30} \times \sqrt{30})R30°$ symmetry on Au(111).[34] The islands are thus crystalline. This crystallinity is corroborated by their uniform height and compact shape. Furthermore, the herringbone reconstruction is visible through the water islands as parallel bright lines (in enhanced contrast Fig. 1a, lower left). The height of the ridges on top of the water islands, as visible in the height profile in Fig. 1c, is of the same order as the height variation on the pristine Au(111) (indicated by arrows in Fig. 1c). The observation of the herringbone reconstruction through the ice islands might be either an electronic or a structural effect, or both. In any case the otherwise flat top supports the crystallinity of the ice islands.

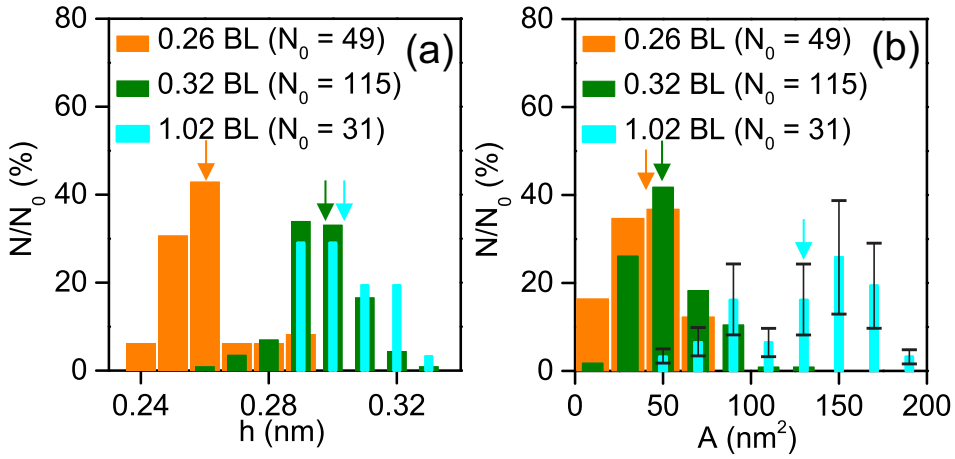

Figure 2: Geometrical characterization of water islands nucleated at (115 ± 5) K for three different coverages: 0.26 BL, 0.32 BL, 1.02 BL; 190 to 280 mV: (a) apparent height histogram (b) area histogram. Arrows point to corresponding mean values.

The apparent height of the islands depends on the applied bias voltage, however, not markedly in the voltage range used here, between 190 mV and 280 mV. In this voltage range, the apparent height is between 0.24 nm and 0.33 nm (Fig. 2a). The height histogram at a coverage of 0.26 BL has its maximum and mean value at (0.26 ± 0.01) nm (orange arrow in Fig. 2a). Note that this apparent height largely underestimates the real height of the water islands at the low voltage of our measurement, because tunneling occurs in their band gap region.[28] For an estimation of the real height, we compare the apparent heights (Fig. 2a) to

the ones of crystalline ice islands grown on Cu(111), where apparent heights were related to real heights via imaging beyond the band gap.[28] The mean in apparent height at 0.26 BL corresponds to crystalline water islands on Cu(111) to a geometric height of 0.86 nm, and thus to two bilayers.[28] This suggests that the real height of most of the islands here is also two water bilayers. At a slightly larger coverage of 0.32 BL, maximum and mean are shifted to larger values. The mean value of the islands increases to (0.30 ± 0.01) nm, corresponding to a geometric height of 1.05 nm on Cu(111) and thus to three bilayers.[28] This apparent height, at a mean of (0.30 ± 0.01) nm is essentially preserved at triple the coverage, a full bilayer equivalent. Regardless of the exact quantitative assignment, the height histogram shows a clear layering and a non-linear step-like increase in height between a quarter and a third of a bilayer.

The area distribution of the water islands is rather broad (Fig. 2b), hardly shifting between 0.26 and 0.32 BL, at a mean area of (40 ± 20) nm^2 at 0.26 BLs and of (50 ± 20) nm^2 at 0.32 BLs. In this coverage range, the islands mainly grow in height but less in lateral dimension. At higher coverage, the islands grow predominantly laterally. The mean area of the water islands at a coverage of 1.02 BL is, at (130 ± 40) nm^2, approximately 3 times larger than the one at 0.32 BL. The area distribution is much broader and, in contrast to the rather uniform area distribution at lower coverage, there seem to be two maxima at 1.02 BL, one at 90 nm^2 and another one at 150 nm^2 (Fig. 2b). Such a distribution is indicative of island growth through coalescence of smaller islands, indicating a certain mobility of the islands as a whole over the surface.[41,42]

Having characterized the water islands geometrically, we now analyse the desorption kinetics of water on pristine Au(111) at increasing coverages. The desorption is, at all investigated coverages, typical for water desorption from noble metal surfaces.[30,38] Typical for TPD of water from noble metals, desorption is initially zero order with a common leading edge and a shift of the desorption maximum to higher temperatures at increasing coverages, with the maxima ranging between 154 K and 161 K as the coverage increases to 0.41 BL

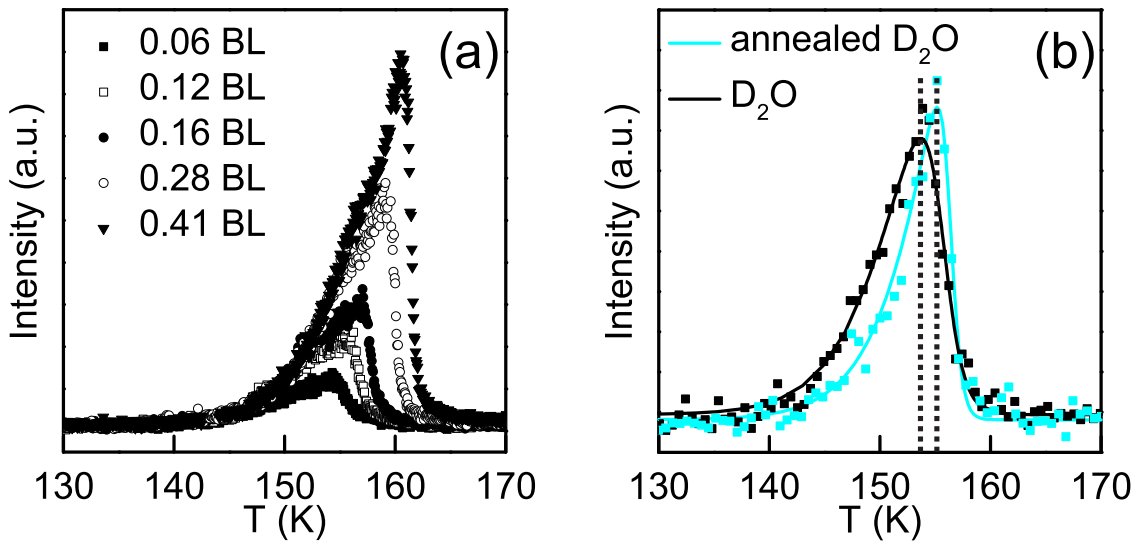

Figure 3: TPD spectra of water adsorbed on Au(111) at 100 K: (a) at increasing coverages (b) different preparations at 0.06 BL: without post-annealing (black squares: experiment, black line: fit) and with post-annealing at 130 K for 15 minutes (grey squares: experiment, grey line: fit). Dashed vertical lines mark maxima as obtained from fitting.

(Fig. 3a). The desorption rate falls away from a zero order behaviour as desorption proceeds, forming a shoulder some Kelvin below the desorption maximum for a 0.41 BL film before the rate increases again at higher temperature. For thick water films a similar decrease in desorption rate is conventionally interpreted as crystallization,[43,44] but a reduced desorption rate can also result from water aggregating into larger islands during annealing.[45] First layer water crystallization already starts at 110 K on Au(111),[34] implying the late appearance of this shoulder is a kinetic effect as the island size distribution changes during annealing. Indeed, the TPD spectrum of as adsorbed water differs from the one of water post-annealed at 130 K for 15 minutes, at same coverage (Fig. 3b). The leading edges and the desorption maxima of the two spectra have the same slope, but are shifted by approximately 2 K towards higher temperatures for the post-annealed water, indicating a similar water binding but a reduced desorption rate. Thus, the observed increase in desorption temperature confirms the interpretation of the shoulders in Fig. 3a and is consistent with crystalline water nanoislands observed by STM at (125 ± 5) K (cf. Fig. 1).

Imaging water in the range of desorption in the TPD spectrum at 146 K modifies the water

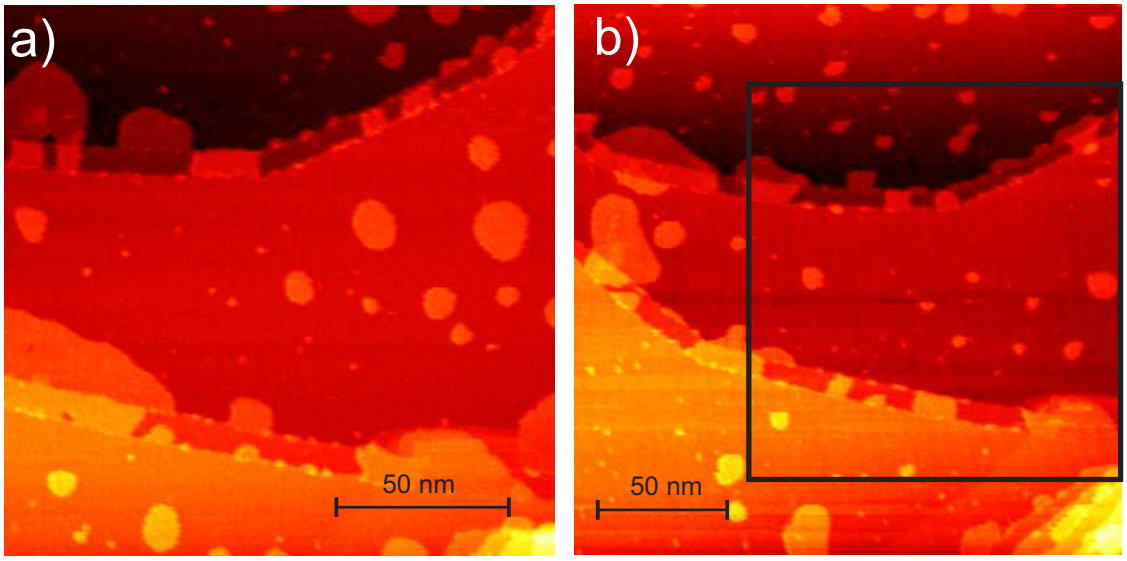

Figure 4: Influence of imaging on water islands at T = (146 ± 1) K: 1.02 BL grown at (115 ± 5) K: Two consecutive STM images of different size imaged 91 s apart; black rectangle in (b) is region scanned in (a). (a) 100 pA, 1540 mV (b) 260 pA, 1540 mV.

islands as demonstrated in Fig. 4. After having recorded Fig. 4a, we scanned a larger region (Fig. 4b). In the scanned region, no large water islands remain (black rectangle in Fig. 4b), though they still exist in the non-scanned region around. Below, we will show that this is different for imaging water on Li precovered Au(111) at the desorption temperature.

Lithium adsorption on Au(111).

Having characterized the water structure and desorption kinetics on pristine Au(111) we now characterize the adsorption of lithium at submonolayer coverage.

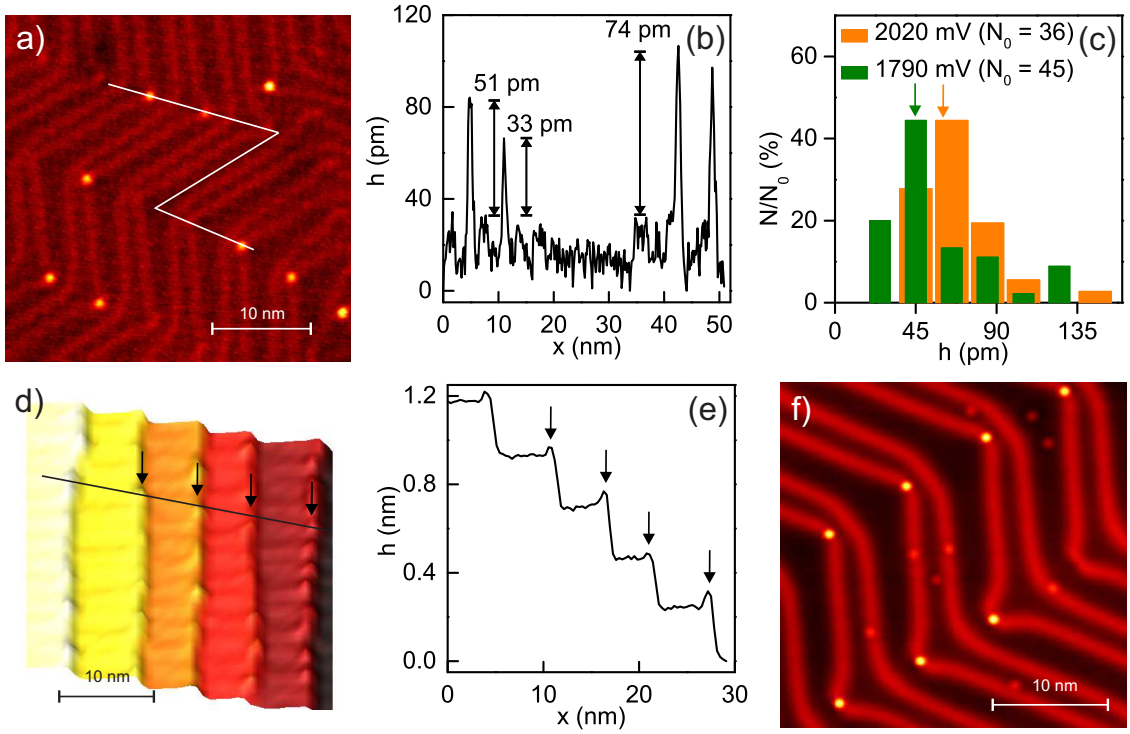

Figure 5: Lithium ions on Au(111): Li visible coverage 0.09 % ML (a,d) and 0.14 % ML (f) adsorbed at (215 ± 5) K: (a) STM image of a terrace region; 80 pA, 1790 mV, T = (129 ± 1) K (b) height profile along line in (a), (c) apparent height histograms of lithium on terraces; arrows point to maxima (d) STM image of a stepped region; 110 pA, 1790 mV, T = (129 ± 1) K (e) profile along line in (d); arrows point to protrusions at the steps (f) STM image at low temperature; 11 pA, -1870 mV, T = (7 ± 1) K.

At tunneling currents between 80 pA to 200 pA, the lithium ions are not visible in the voltage range between ∼1600 mV and ∼-1600 mV. They are imaged as protrusions at voltages between 1600 mV to 2700 mV as well as at -1600 mV (Fig. 5).

At both investigated coverages, lithium ions are imaged exclusively at either the elbow sites of the herringbone reconstruction (Fig. 5a,b) or steps (Fig. 5d,e). There is no statistically relevant preference for the x-elbow or y-elbow sites of the herringbone reconstruction. Concerning the adsorption at steps, work function changes suggested a similar preference of

lithium to step edges on Ni(775), prior to occupation of terrace sites at a Li coverage higher than 0.08 ML.[46] As the number of imaged lithium ions does not increase linearly with increasing deposition as soon as all the elbow sites are occupied, we propose that lithium ions, that are not bound to elbow sites or at stepped region, are mobile at our measurement temperatures above 110 K. To prove this point, we measured lithium on Au(111) at a low temperature of 7 K to suppress this mobility. Indeed, at this low temperature, lithium ions are imaged not only at the elbow sites, but also randomly distributed between them (Fig. 5f). Therefore, we conclude that the Li coverages used in our experiments below are in fact higher than the visible coverage.

The apparent height of the lithium ions on terrace region is estimated by measuring the height difference between lithium ions at elbow sites and not occupied elbow sites (Fig. 5b). 87 % of the protrusions have an apparent height of (45 ± 12) pm above the elbow site at 1790 mV (Fig. 5c). The apparent height of the Li at step edges is (45 ± 10) pm at 1790 mV and thus identical to the one on terraces. Note that the apparent height maximum of the height histogram is at (65 ± 15) pm at 2020 mV. The 50 % higher apparent height value of the lithium ions at only 200 mV higher voltage suggests that the imaging at above -1600 mV is related to some electronic state. It further allows to discriminate the Li ions from some unavoidable impurities of larger apparent height, whose apparent height remain at approximately the same value at the two voltages presented. The apparent height of the Li at the elbow sites imaged at -1870 mV at low temperature fits, at (60 ± 20) pm, quite well to the values above (Fig. 5f). Most importantly, the rather uniform size suggests that the Li exists mainly as monomers and is thus ionic.

Water adsorption on lithium precovered Au(111).

Having characterized water and lithium separately, we now investigate the influence of the lithium ions on the binding energy of water by comparing the TPD spectra after water adsorption on the pristine surface, presented in Fig. 3, to the ones after adsorption on a Li

precovered Au(111), both at 110 K (Fig. 6). Note that no hydroxide was detected in the TPD spectra; an evidence that the water does not dissociate, but adsorbs molecularly also in the case of Li precovered Au(111).

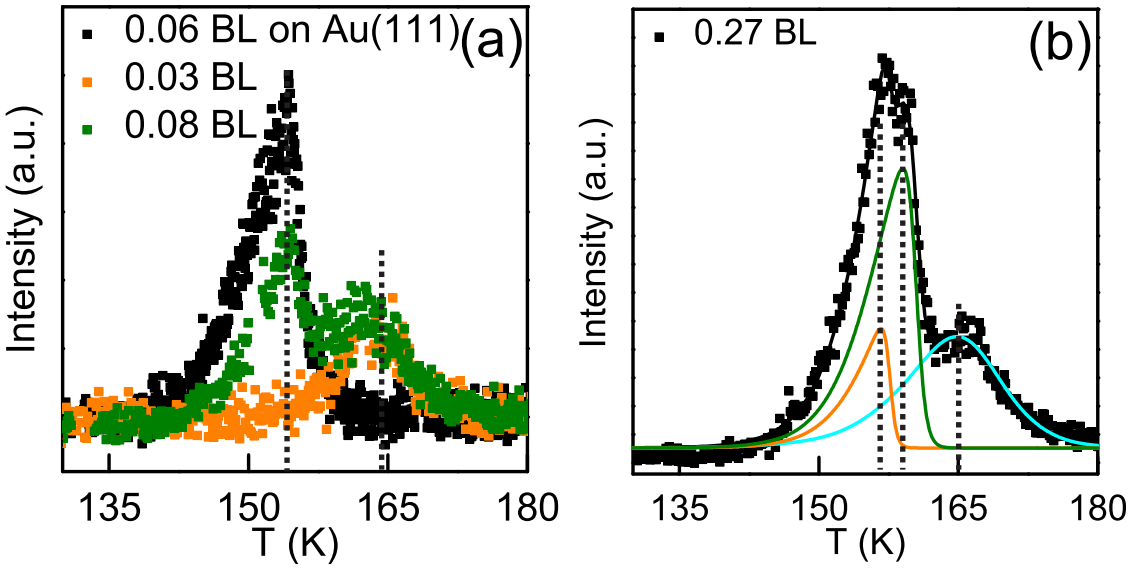

Figure 6: TPD spectra of water on Li precovered Au(111) adsorbed at 110 K for different water coverages, dashed vertical lines through maxima determined by fitting: (a) 0.03 BL (orange squares) and 0.08 BL (green squares) as compared to 0.06 BL water on pristine Au(111) (black squares; reproduced from Fig. 3a), (b) 0.27 BL (black squares) with fits of three maxima (solid line); black line is sum of fits.

There is only one symmetric maximum at 164 K in the TPD spectrum from the Li precovered surface at the lowest investigated water coverage of 0.03 BL (orange squares in Fig. 6a). The TPD spectrum at 0.08 BL water coverage exhibits a maximum of similar shape at 164 K, and a further maximum at 154 K (green squares in Fig. 6a). As the maximum at 164 K has no equivalence in the spectrum from the pristine surface at 0.06 BL water coverage (black squares in Fig. 6a), it must result from water bound to lithium ions. Thus, all water molecules are influenced by the lithium ions at 0.03 BL coverage. The similar temperature and shape of the desorption maximum at 164 K at 0.08 BL suggest that it corresponds likewise to water whose binding is directly affected by the lithium. We conclude that the amount of water affected by lithium ions is limited only. With increasing water coverages more and more water is not influenced by them and is bound in the same way as water on

the pristine surface. A similar stabilizing effect on only a fraction of the water was reported before for 0.08 ML of potassium on Pt(111) by TPD.[17]

To prove this point, we fit the TPD spectrum at 0.27 BL on the Li precovered surface by three maxima (Fig. 6b). The sum of the resulting fits gives an excellent description of the experimental data (black line). Hereby fit 1 at 157 K and fit 2 at 159 K exhibit a zero order desorption kinetic as water on the pristine surface (cf. Fig. 3a), the peak 3 at 165 K has a very different, rather symmetric shape suggesting first order desorption kinetics. While the zeroth order desorption of water from the pristine metal reflects that the water-water binding is stronger than the water-metal binding, first order desorption indicates stronger (non-dissociative) binding, here not to the surface itself, but to the surface adsorbate Li. The difference in temperature of 10 K between 154 K and 164 K at 0.08 BL water coverage on Li precovered Au(111) corresponds to a difference in desorption energy of (2.7 $\pm$ 0.3) kJ/mol or 0.028 eV under the assumption that the desorption can be described by the Redhead approximation.[47]

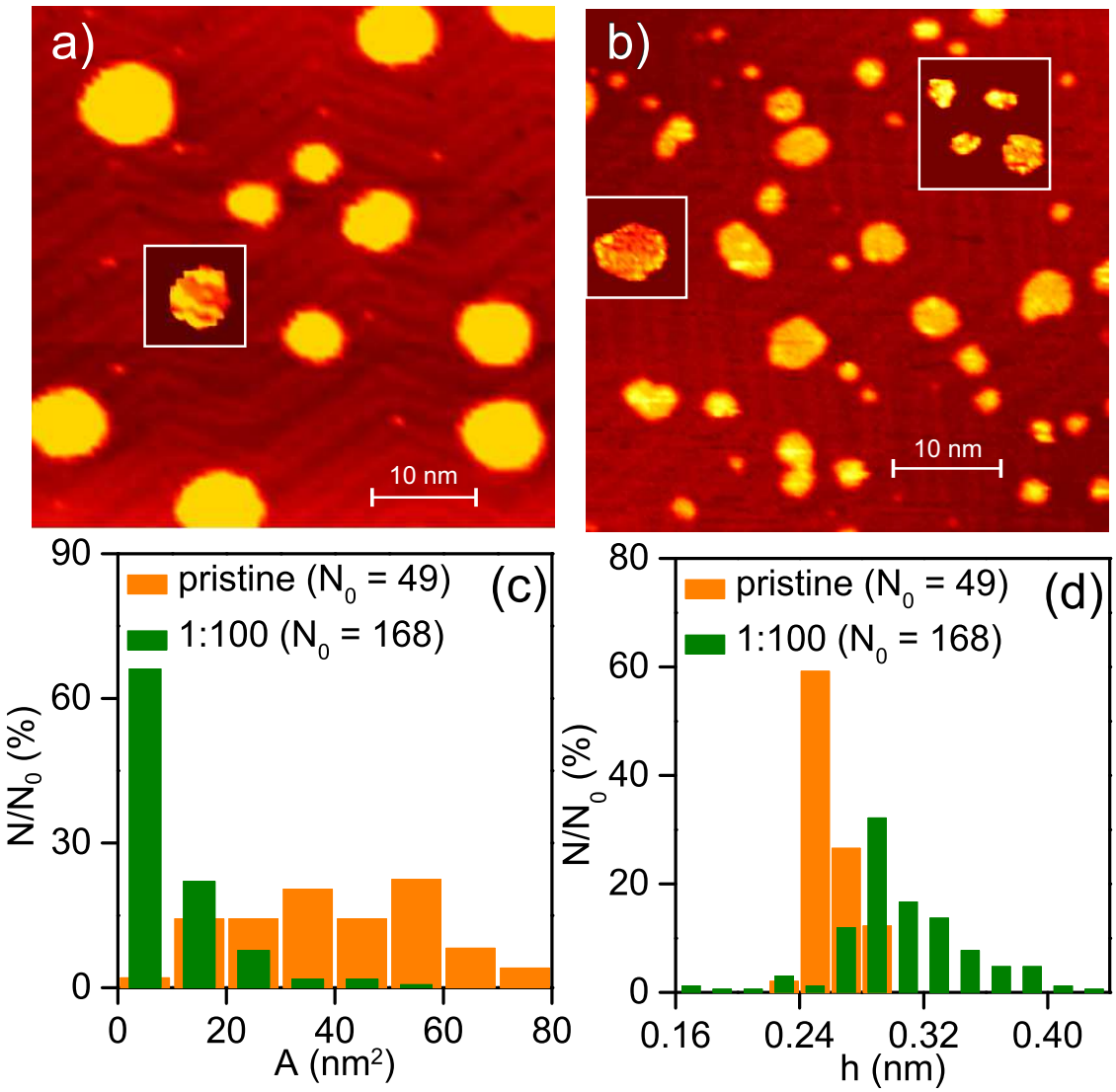

Figure 7: Effect of Li precoverage on water structures adsorbed at (115 ± 5) K: STM images (a, b) of water islands on (a) pristine Au(111); water coverage 0.26 BL; contrast is enhanced in rectangle, 60 pA, 280 mV, T = (125 ± 1) K (b) Li precovered Au(111); 0.23 BL, Li visible coverage of 0.15 % ML, ratio of Li:D_2O 1:100, adsorbed at (215 ± 5) K; contrast is enhanced in rectangles, 70 pA, 1790 mV, T = (122 ± 1) K (c) area histogram; on pristine Au(111) reproduced from Fig. 2b (d) apparent height histogram; on pristine Au(111) reproduced from Fig. 2a at double bin size; voltages as in images; for high-resolution images of insets see supporting information.

While the binding energy of only very few water molecules is affected by the Li ions, we will demonstrate now that the effect on structure is much more extended. To this aim, we compare water islands on pristine Au(111) (Fig. 7a) to those on Li precovered Au(111) with a

visible coverage of 0.15 % ML Li (Fig. 7b), a ratio of Li:D_2O 1:100, respectively. The presence of this small amount of Li ions, which affects less than 0.06 ML of the water according to our TPD study, changes the water structures both qualitatively and quantitatively in four ways. First, the shape of the water islands on the Li precovered surface is less compact and more irregular than on pristine Au(111). Second, the herringbone reconstruction on top of the water islands on pristine Au(111) is absent on top of the water island on an Li precovered Au(111) (cf. enhanced contrast in Fig. 7a to 7b). Third, the number of water islands on the Li precovered surface is larger, at smaller size. Indeed, the area distribution of water islands on Li precovered surface is much narrower and shifted to lower values than the one for the water islands on the pristine surface (Fig. 7c). At approximataly the same water coverage of 0.26 BL the median value is on the Li precovered surface, at 11 nm^2, only a quarter of the 39 nm^2 on the pristine surface. Note that the water islands on the Li precovered surface at higher Li coverage (cf. Fig. 5f and 7b) do not only nucleate on the Li ions at the elbow sites of the herringbone reconstruction, but also on the other, randomly distributed Li ions on Au(111). Fourth, whereas water islands on the pristine surface are characterized by a uniform height, the water islands on the Li precovered Au(111) have a larger variation (cf. Fig. 7a to 7b). The height distribution of water islands on the Li precovered surface is indeed very broad, ranging from 0.17 nm to 0.43 nm (Fig. 7d), in contrast to the height distribution of water islands on pristine Au(111), ranging from 0.23 nm and 0.29 nm only (Fig. 7d). This much broader height distribution shows that the lithium ions break the clear layering of water identified above. This demonstrates for the first time the effect of a kosmotrope in real space.

As shown above by TPD experiments, the water molecules at the deposition temperature of (115 $\pm$ 5) K are mobile and nucleate at lithium ions. This explains, why the number of water islands on the Li precovered surface is much larger than on the pristine Au(111), leading to smaller islands on average.

The higher binding energy deduced from the TPD spectra above is reflected in an altered

imaging characteristics of the water islands. Whereas unperturbed imaging for crystalline ice structures on the pristine surface is only possible at bias voltages below ∼300 mV, water structures on the Li precovered surface can be imaged at voltages up to ∼2.8 V.

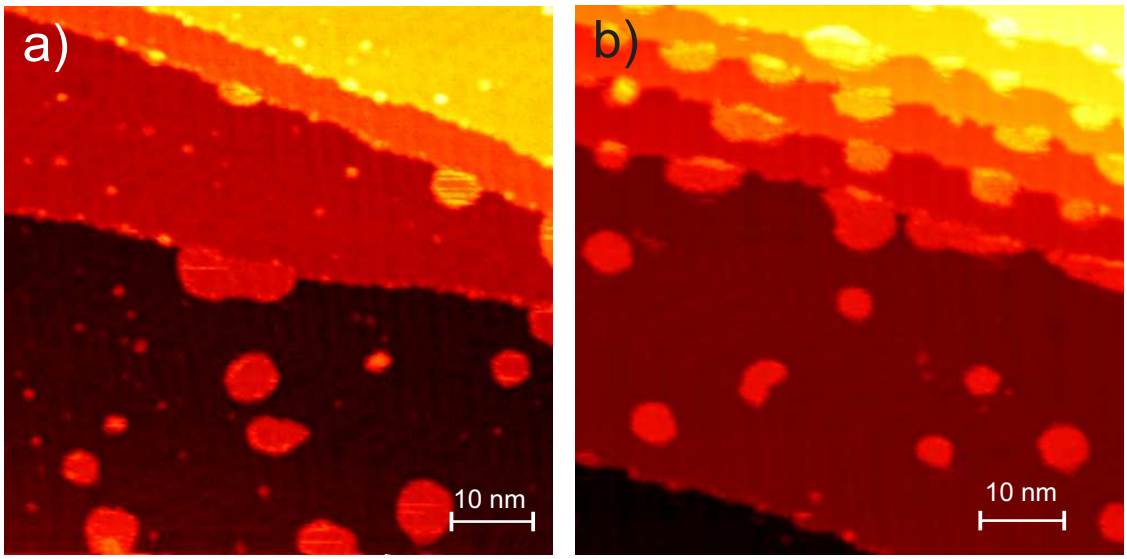

Figure 8: Dependence of water structures at (136 ± 1) K on Li coverage: water adsorbed at (115 ± 5) K, lithium adsorbed at (215 ± 5) K: STM images at (a) 0.15 % ML visible Li coverage, 0.23 BL water coverage; 60 pA, 2360 mV (b) 0.09 % ML visible Li coverage, 0.26 BL water coverage; 100 pA, 1580 mV.

Furthermore, the water on the pristine surface cannot be imaged at elevated temperature, see above, but this is possible for water on the Li precovered surface. This allows us to investigate their geometry up to desorption temperature. Between (122 ± 1) K (Fig. 7b) and (136 ± 1) K the size distribution changed, at 0.15 % ML visible Li coverage (Fig. 8a). While still covering a similar size range up to 80 nm^2 (apart from one exception), the mean has increased from 11 nm^2 to 30 nm^2. As no desorption of water takes place at this temperature (c.f. TPD Fig. 6a), the broadened distribution results from a substantial redistribution of the adsorbates. Thus, the water desorbs as water on pristine Au(111) from each island leading to a maximum at the same temperature until the D_2O/Li ratio reduces to a critical point where the stability of the water is changed sufficiently to slow water desorption and form a second peak at higher temperature. At both Li coverages, there are, at 136 K, large water islands on stepped and on terrace regions (Fig. 8a and 8b). However, the number of small water islands on the terrace is substantially reduced at a visible coverage of 0.09 % ML.

Possibly,the solvated lithium ions at this lower Li coverage are mainly adsorbed at the step edges and only rarely on the terrace region as in the case of lithium on the pristine surface.

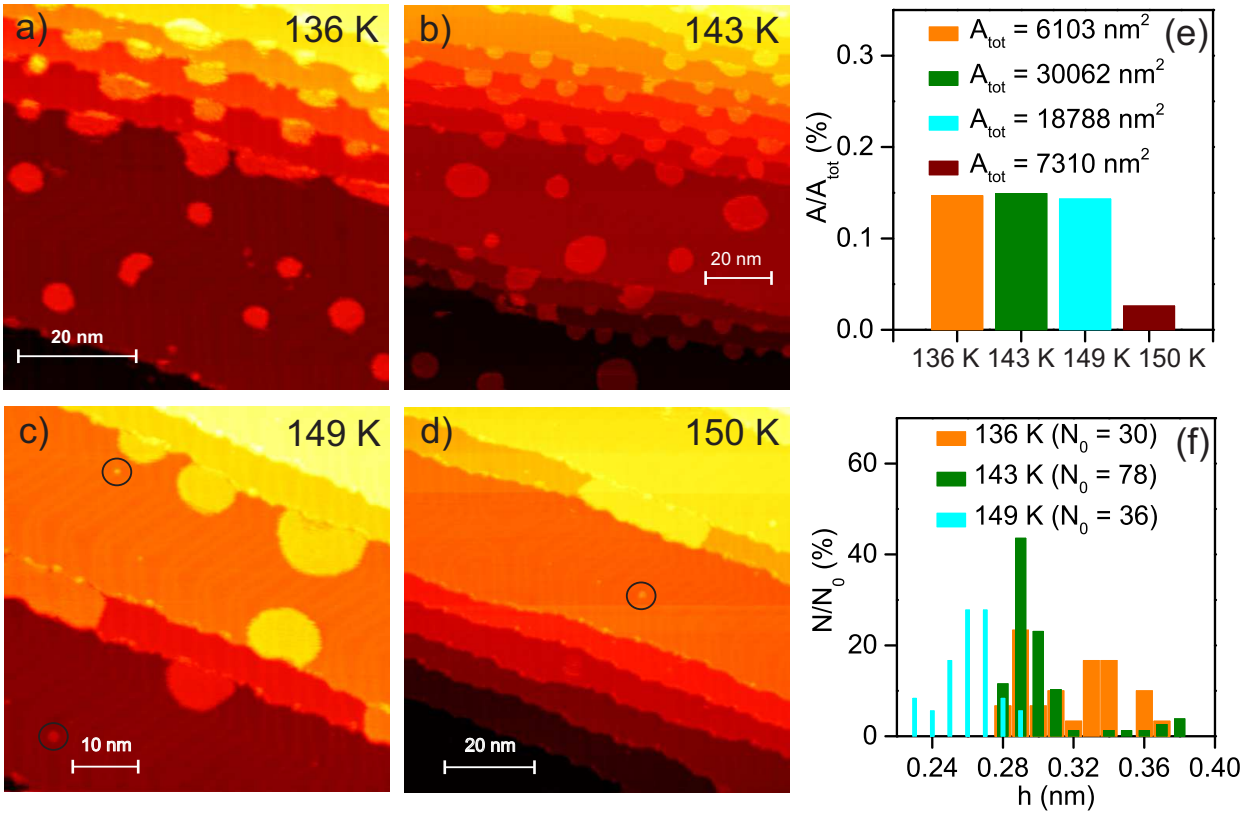

Figure 9: Desorption of water from Li precovered Au(111) in a temperature range between 136 K and 150 K; 0.09 % ML visible Li coverage adsorbed at (215 ± 5) K, 0.23 BL water coverage adsorbed at (115 ± 5) K: (a-d) STM images at increasing temperature (a) T = (136 ± 1) K (b) T = (143 ± 1) K (c) T = (149 ± 1) K (d) T = (150 ± 1) K (e) area covered by water islands at 136 K, 143 K, 149 K and 150 K (f) apparent height histogram; for scanning voltages of 1360 mV (136 K), 1960 mV (143 K), 2590 (149 K) and 2840 mV (150 K). Circles in (c) and (d) indicate solvated lithium ions. Tunnel parameters: (a) 20 pA, 1360 mV (b) 120 pA, 1960 mV (c) 120 pA, 2590 mV (d) 130 pA, 2840 mV.

Finally, we follow the desorption of water from Li precovered Au(111), at a visible coverage of 0.09 % ML in real space, at several temperatures between 136 K and 150 K, i.e. up to the maximum in the TPD spectrum of water on the pristine surface (Fig. 9a-d). Large water islands exist up to 149 K at step edges and at 150 K between step edges. On the terrace region, only some small dots can be found (circle in Fig. 9d) at the higher temperature of 150 K (Fig. 9d). In contrast to the imaging of water islands on the pristine surface (cf. Fig. 4),

the water islands are not perturbed by the imaging process, even at high voltages between ∼1400 mV and ∼2800 mV. A further confirmation of the increase of water binding energy by the lithium ions.

The covered area does not change up to 149 K, but decreases rapidly at 150 K (Fig. 9e). This is surprising as the TPD spectra suggest already desorption at the two lower temperatures. However, the apparent height of the water islands decreases with increasing temperature (Fig. 9f). The mean of the apparent height reduces from (0.33 ± 0.04) nm at 136 K to (0.26 ± 0.01) nm at 149 K (Fig. 9f). For experimental reasons, the images are taken at higher voltage for higher temperatures. As such an increase in voltage should lead to an increase of apparent height, the reduction in apparent height is even larger than suggested by this histogram. Thus water does not exclusively desorb from the step edges, which would lead to a decrease in covered area, but from all the island surface. This is consistent with the zeroth order desorption peak at 154 K, which suggests multilayer desorption. The stabilizing effect of Li thus facilitates to identify the desorption places of the water.

Conclusions

By combining TPD with STM measurements, we demonstrate the significant influence of a kosmotropic ion on the structure of water nanoislands. On Au(111), water adsorbs molecularly regardless of the presence of lithium monomers at Li coverages below 0.15 % ML. TPD spectra suggest that only a fraction of water is more strongly bound by the ions. With increasing water coverage, more and more water desorbs as from the pristine surface. However, STM measurements reveal that all water molecules are affected by the lithium ions. In this case, the water nanoislands exhibit no clear layering in contrast to the ones on the pristine surface. Moreover, STM identifies the desorption sites of the water molecules, surprisingly, from the top layer of the nanoislands. Our results thus offer a real-space image of the structure changes to water by kosmotropic ions.

Our study suggests a similar effect of other kosmotropic ions on the structure of water nanoislands, although their larger size might influence the nanoislands geometry and distribution. In a broader sense, the influence of the surface is expected to be small, because of the major influence of lithium ions on the structure of supported water nanoislands. Thus our results could be correlated to solvation of alkali metal ions by water molecules in solution.

Supporting Information

The supporting information provides high-resolution images of Figures in the main manuscript.

Acknowledgement

This work is funded by the Deutsche Forschungsgemeinschaft (DFG, German Research Foundation) under Germany's Excellence Strategy - EXC-2033 - Projektnummer 390677874. The authors thank Chanfang Lin for the experimental support.

References

(1) Suo, L.; Borodin, O.; Gao, T.; Olguin, M.; Ho, J.; Fan, X.; Luo, C.; Wang, C.; Xu, K. "Water-in-salt" electrolyte enables high-voltage aqueous lithium-ion chemistries. *Science* **2015**, *350*, 938–943.

(2) Kanan, M. W.; Nocera, D. G. In Situ Formation of an Oxygen-Evolving Catalyst in Neutral Water Containing Phosphate and Co^{2+}. *Science* **2008**, *321*, 1072–1075.

(3) Boyd, S.; Augustyn, V. Transition metal oxides for aqueous sodium-ion electrochemical energy storage. *Inorg. Chem. Front.* **2018**, *5*, 999–1015.

(4) Arijs, I. Stratospheric ion chemistry: Present understanding and outstanding problems. *Planet. Space Sci.* **1992**, *40*, 255–270.

(5) Lo Nostro, P.; Ninham, B. W. Hofmeister Phenomena: An Update on Ion Specificity in Biology. *Chem. Rev.* **2012**, *112*, 2286–2322.

(6) Ke, H.; Lisy, J. M. Influence of hydration on ion-biomolecule interactions: M^+(indole)$(H_2O)_n$ (M = Na, K; n = 3-6). *Phys. Chem. Chem. Phys.* **2015**, *17*, 25354–25364.

(7) Varma, S.; Rempe, S. B. Coordination numbers of alkali metal ions in aqueous solution. *Biophys. Chem.* **2006**, *124*, 192–199.

(8) Mähler, J.; Persson, I. A Study of the Hydration of the Alkali Metal Ions in Aqueous Solution. *Inorg. Chem.* **2012**, *51*, 425–438.

(9) Waluyo, I.; Nordlund, D.; Bergmann, U.; Schlesinger, D; Pettersson, L. G. M.; Nilsson, A. A different view of structure-making and structure-breaking in alkali halide aqueous solutions through x-ray absorption spectroscopy. *J. Phys. Chem.* **2014**, *140*, 244506.

(10) Schienbein, P.; Schwaab, G.; Forbert, H.; Havenith, M.; Marx, D. Correlations in the Solute-Solvent Dynamics Reach Beyond the First Hydration Shell of Ions. *J. Phys. Chem. Lett.* **2017**, *8*, 2373–2380.

(11) Džidić, I.; Kebarle, P. Hydration of the Alkali Ions in the Gas Phase. Enthalpies and Entropies of Reactions $M^+(H_2O)_{n-1} + H_2O = M^+(H_2O)_n$. *J. Phys. Chem.* **1970**, *74*, 1466–1474.

(12) Blades, A. T.; Jayaweera, P., Ikonomou, M. G.; Kebarle, P. Studies of alkaline earth and transition metal M^{++} gas phase ion chemistry. *J. Chem. Phys.* **1990**, *92*, 5900.

(13) Beyer, M. K. Hydrated metal ions in the gas phase. *Mass Spectrom. Rev.* **2007**, *26*, 517–541.

(14) Zatula, A.; Ryding, M. J.; Andersson, P. U.; Uggeru, E. Proton mobility and stability

of water islands containing alkali metal ions. *Int. J. Mass Spectrom.* **2012**, *330-332*, 191–199.

(15) Ke, H.; van der Linde, C.; Lisy, J. M. Insights into the Structures of the Gas-Phase Hydrated Cations $M^+(H_2O)_nAr$ (M = Li, Na, K, Rb, and Cs; n = 3-5) Using Infrared Photodissociation Spectroscopy and Thermodynamic Analysis. *J. Phys. Chem. A* **2015**, *119*, 2037–2051.

(16) Doering, D. L.; Semancik, S.; Madey, T. E. Coadsorption of water and sodium on the Ru(001) surface. *Surf. Sci.* **1983**, *133*, 49–70.

(17) Kizhakevariam, N.; Villegas, I.; Weaver, M. J. Infrared Spectroscopy of Model Electrochemical Interfaces in Ultrahigh Vacuum: Roles of Adsorbate and Cation Double-Layer Hydration in the Pt(111)-Carbon Monoxide Aqueous System. *J. Phys. Chem.* **1995**, *99*, 7677–7688.

(18) Ito, M. Structures of water at electrified interfaces: Microscopic understanding of electrode potential in electric double layers on electrode surfaces. *Surf. Sci. Rep.* **2008**, *63*, 329–389.

(19) Meyer, M.; Agarwal, I.; Wolf, M.; Bovensiepen, U. Ultrafast electron dynamics at water covered alkali adatoms adsorbed on Cu(111). *Phys. Chem. Chem. Phys.* **2015**, *17*, 8441.

(20) Peng, J.; Cao, D.; He, Z.; Guo, J.; Hapala, P.; Ma, R.; Cheng, B.; Chen, J.; Xie, W. J.; Li, X.-Z., et. al. The effect of hydration number on the interfacial transport of sodium ions. *Nature* **2018**, *557*, 701–705.

(21) Dang, L. X.; Rice, J. E.; Caldwell, J.; Kollman, P. A. Ion Solvation in Polarizable Water: Molecular Dynamics Simulations. *J. Am. Chem. Soc.* **1991**, *113*, 2481–2486.

(22) Pluhařová, E.; Mason, P. E.; Jungwirth, P. Ion Pairing in Aqueous Lithium Salt So-

lutions with Monovalent and Divalent Counter-Anions. *J. Phys. Chem. A* **2013**, *117*, 11766–11773.

(23) Krekeler, C.; Hess, B.; Site, L. D. Density functional study of ion hydration for the alkali metal ions (Li^+,Na^+,K^+) and the halide ions (F^-,Br^-,Cl^-). *J. Chem. Phys.* **2006**, *125*, 054305.

(24) Rao, J. S.; Dinadayalane, T. C.; Leszczynski, J.; Sastry, G. N. Comprehensive Study on the Solvation of Mono- and Divalent Metal Cations: Li^+, Na^+, K^+, Be^{2+}, Mg^{2+} and Ca^{2+}. *J. Phys. Chem. A* **2008**, *112*, 12944–12953.

(25) Mignon, P.; Ugliengo, P.; Sodupe, M.; Hernandez, E. R. Ab initio molecular dynamics study of the hydration of Li^+, Na^+ and K^+ in a montmorillonite model. Influence of isomorphic substitution. *Phys. Chem. Chem. Phys.* **2010**, *12*, 688–697.

(26) Mehlhorn, M.; Morgenstern, K. Faceting during the Transformation of Amorphous to Crystalline Ice. *Phys. Rev. Lett.* **2007**, *99*, 246101.

(27) Thürmer, K.; Bartelt, N. C. Growth of multilayer ice films and the formation of cubic ice imaged with STM. *Phys. Rev. B* **2008**, *77*, 195425.

(28) Mehlhorn, M.; Morgenstern, K. Height analysis of amorphous and crystalline ice structures on Cu(111) in scanning tunneling microscopy. *New J. Phys.* **2009**, *11*, 093015.

(29) Maier, S.; Lechner, B. A. J.; Somorjai, G. A.; Salmeron, M. Growth and Structure of the First Layers of Ice on Ru(0001) and Pt(111). *J. Am. Chem. Soc.* **2016**, *138*, 3145–3151.

(30) Hodgson, A.; Haq, S. Water adsorption and the wetting of metal surfaces. *Surf. Sci. Rep.* **2009**, *64*, 381–451.

(31) Carrasco, J.; Hodgson, A.; Michaelides, A. A molecular perspective of water at metal interfaces. *Nat. Mater.* **2012**, *11*, 667–674.

(32) Gawronski, H.; Morgenstern, K.; Rieder, K.-H. Electronic excitation of ice monomers on Au(111) by scanning tunneling microscopy. *Eur. Phys. J. D* **2005**, *35*, 349–353.

(33) Stacchiola, D.; Park, J. B.; Liu, P.; Ma, S.; Yang, F.; Starr, D. E.; Muller, E.; Sutter, P.; Hrbek, J. Water Nucleation on Gold: Existence of a Unique Double Bilayer. *J. Phys. Chem. C* **2009**, *113*, 15102–15105.

(34) Corem, G.; Kole, P. R.; Zhu, J.; Kravchuk, T.; Manson, J. R.; Alexandrowicz, G. Ordered H_2O Structures on a Weakly Interacting Surface: A Helium Diffraction Study of H_2O/Au(111). *J. Phys. Chem. C* **2013**, *117*, 23657–23663.

(35) Marcus, Y. Effect of Ions on the Structure of Water: Structure Making and Breaking. *Chem. Rev.* **2009**, *109*, 1346–1370.

(36) Graham, A. P.; Toennies, J. P. Helium-atom diffraction study of the submonolayer structures of sodium on Cu(001). *Phys. Rev. B* **1997**, *56*, 15378–15390.

(37) Politano, A.; Chiarello, G.; Benedek, G.; Chulkov, E. V.; Echenique, P. M. Vibrational spectroscopy and theory of alkali metal adsorption and co-adsorption on single-crystal surfaces. *Surf. Sci. Rep.* **2013**, *68*, 305–389.

(38) Kay, B. D.; Lykke, K. R.; Creighton, J. R.; Ward, S. J. The influence of adsorbate-absorbate hydrogen bonding in molecular chemisorption: NH_3, HF, and H_2O on Au(111). *J. Chem. Phys.* **1989**, *91*, 5120–5121.

(39) Lin, C.; Avidor, N.; Corem, G.; Godsi, O.; Alexandrowicz, G.; Darling, G. R.; Hodgson, A. Two-Dimensional Wetting of a Stepped Copper Surface. *Phys. Rev. Lett.* **2018**, *120*, 076101.

(40) Horcas, I.; Fernández, R. WSXM: A software for scanning probe microscopy and a tool for nanotechnology. *Rev. Sci. Instrum.* **2007**, *78*, 013705.

(41) Kuipers, L.; Palmer, R. E. Influence of island mobility on island size distributions in surface growth. *Phys. Rev. B* **1996**, *53*, R7646.

(42) Heidorn, S.-C.; Bertram, C.; Morgenstern, K. The fractal dimension of ice on the nanoscale. *Chem. Phys. Lett.* **2016**, *665*, 1–5.

(43) Yuan, C.; Smith, R. S.; Kay, B. D. Surface and bulk crystallization of amorphous solid water films: Confirmation of "top-down" crystallization. *Surf. Sci.* **2016**, *652*, 350–354.

(44) Smith, R. S.; Huang, C.;. Wong, E. K. L; Kay, B. D. Desorption and crystallization kinetics in nanoscale thin films of amorphous water ice. *Surf. Sci.* **1996**, *367*, L13–L18.

(45) Haq, S.; Hodgson, A. Multilayer Growth and Wetting of Ru(0001). *J. Chem. Phys. C* **2007**, *111*, 5946–5953.

(46) Mundt, C.; Benndorf, C. H_2O adsorption on alkali (Li, Na and K) precovered Ni(775). *Surf. Sci.* **1998**, *405*, 121–137.

(47) King, D. A. Thermal desorption from metal surfaces: A review. *Surf. Sci.* **1975**, *47*, 384–402.

TOC Graphic